THE JOURNAL OF
PHYSICAL CHEMISTRY C

Article

pubs.acs.org/JPCC

Optimizing the Energy Offset between Dye and Hole-Transporting Material in Solid-State Dye-Sensitized Solar Cells

Christian T. Weisspfennig,[†] Michael M. Lee,[†] Joël Teuscher,[†] Pablo Docampo,[†] Samuel D. Stranks,[†] Hannah J. Joyce,[†] Hermann Bergmann,[‡] Ingmar Bruder,[‡] Dmitry V. Kondratuk,[§] Michael B. Johnston,[†] Henry J. Snaith,[†] and Laura M. Herz*,[†]

[†]Clarendon Laboratory, Department of Physics, University of Oxford, Parks Road, Oxford OX1 3PU, United Kingdom

[‡]BASF SE, 67056 Ludwigshafen, Germany

[§]Dyson Perrins Laboratory, Department of Chemistry, University of Oxford, South Parks Road, Oxford OX1 3QY, United Kingdom

Supporting Information

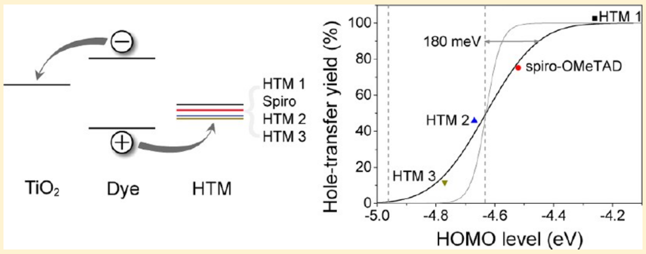

ABSTRACT: The power-conversion efficiency of solid-state dye-sensitized solar cells can be optimized by reducing the energy offset between the highest occupied molecular orbital (HOMO) levels of dye and hole-transporting material (HTM) to minimize the loss-in-potential. Here, we report a study of three novel HTMs with HOMO levels slightly above and below the one of the commonly used HTM 2,2′,7,7′-tetrakis(*N*,*N*-di-*p*-methoxyphenylamino)-9,9′-spirobifluorene (spiro-OMeTAD) to systematically explore this possibility. Using transient absorption spectroscopy and employing the ruthenium based dye Z907 as sensitizer, it is shown that, despite one new HTM showing a 100% hole-transfer yield, all devices based on the new HTMs performed worse than those incorporating spiro-OMeTAD. We further demonstrate that the design of the HTM has an additional impact on the electronic density of states present at the TiO_2 electrode surface and hence influences not only hole- but also electron-transfer from the sensitizer. These results provide insight into the complex influence of the HTM on charge transfer and provide guidance for the molecular design of new materials.

INTRODUCTION

Over the last 20 years, dye-sensitized solar cells (DSSCs) have emerged as a promising alternative to conventional photovoltaic techniques due to the use of cheap materials and low production costs.[1,2] DSSCs separate the processes of light absorption, electron- and hole transport between three different materials. Light is absorbed by a dye which transfers the electrons into the conduction band of a mesoporous metal oxide, usually TiO_2.[3,4] The dye is then regenerated by a hole-transporting material (HTM) which is infiltrated into the mesoporous network and transports the hole to the respective electrode. DSSCs have conventionally incorporated an iodide/triiodide (I^-/I_3^-) liquid electrolyte as the HTM. However, concerns over the solvent leakage and corrosion from the iodide/triiodide redox couple have led to the development of alternatives, such as cobalt complex redox mediators and solid-state HTMs.[2,5] One of the most widely used solid-state HTMs is 2,2′,7,7′-tetrakis(*N*,*N*-di-*p*-methoxyphenylamino)-9,9′-spirobifluorene (spiro-OMeTAD). While DSSCs employing cobalt complex redox mediators have achieved power-conversion efficiencies in excess of 12%,[6] solid-stated DSSCs have reached values of up to 7.2%.[7,8] It has been proposed that incomplete filling of the pores and the low charge carrier mobility of spiro-OMeTAD on the order of 10^{-4} cm^2 $V^{-1}s^{-1}$ are the limiting factors, leading to the difference in power-conversion efficiencies.[9−12] The current optimized device thickness of only 2 μm thus appears to mark the trade-off between light absorption and charge collection.[13] Recently, however, it was shown that the pore-filling fraction required for optimized performance can be achieved with spiro-OMeTAD for thicknesses up to 5 μm[14] suggesting that pore filling may not have to be the final limiting factor. It may also be possible to improve the efficiency of solid-state HTMs by minimizing the energy offset between the HOMO levels of dye and HTM, thus, reducing the loss-in-potential. While the heterogeneity of the energy levels requires a certain offset to efficiently drive the hole-transfer process,[15,16] spiro-OMeTAD might still leave room for improvement.[17] It is estimated that an overpotential of 0.2 eV should be sufficient for near-unity hole regeneration.[2]

Here, we compare three novel triarylamine type hole-transporting materials with similar, but varying, HOMO levels to spiro-OMeTAD to systematically explore the possibility of reducing the overpotential and improving the power-conversion efficiency. Using transient absorption spectroscopy and employing the standard ruthenium sensitizing dye Z907,[18] we show that the hole-transfer yield of spiro-OMeTAD is

Received: June 10, 2013
Revised: August 27, 2013
Published: September 3, 2013

approximately 75%. In addition, we find that all devices based on the new HTMs performed worse than those incorporating spiro-OMeTAD. While the difference for two of the novel HTMs can be explained by a lower hole-transfer yield, one HTM shows a hole-transfer yield of approximately 100%, and hence, other factors must play a role. Using scanning electron microscopy (SEM) imaging, we demonstrate that all HTMs reach a similar and sufficiently high pore-filling fraction and conclude that observed differences in power-conversion efficiency are not caused by inferior pore filling. Instead, transient photovoltage-photocurrent measurements show that the new HTMs induce a shift of the TiO_2 surface potential toward higher values leading to less efficient electron transfer from sensitizer to TiO_2. Overall, our study shows that changes in molecular design of the HTM can have a complex impact on charge transfer from the dye sensitizer, both for transfer of holes to the HTM and electrons to the TiO_2 electrode.

■ EXPERIMENTAL SECTION

The following procedure was performed for fabrication of samples for device measurements. Fluorine doped tin oxide (FTO) coated glass (Pilkington TEC 15) 15 Ω/sq was patterned by etching with zinc powder and 2 M HCl diluted in Milli-Q water. The etched substrate was then cleaned with 2% Hellmanex detergent diluted in Milli-Q water, rinsed with Milli-Q water, acetone and ethanol and finally dried with clean dry air. The substrate underwent an oxygen plasma treatment for 5 min prior to spray pyrolysis of compact titanium dioxide, TiO_2. A thin layer of compact TiO_2 of roughly 100 nm was formed through spray pyrolysis of titanium diisopropoxide bis(acetylacetonate) diluted in anhydrous ethanol at a volumetric ratio of 1:10 using air as a carrier gas. Prior to the formation of the titania mesostructure, the substrate underwent an oxygen plasma treatment for 1 min. One μm thick TiO_2 was formed by spin coating TiO_2 paste (DSL 18-NRT, Dyesol) diluted in anhydrous ethanol at 1.5:1 by weight at 2000 rpm (spin coating was preferred to screen printing or doctor blading due to greater control of mesostructure thickness). The freshly cast layer was then sintered in air at 550 °C. The substrates were immersed in a bath of $TiCl_4$ at a concentration of 15 mM for 1 h at 70 °C, followed by rinsing in Milli-Q water and heating to 550 °C and cooled to 70 °C. Once substrates reached 70 °C, they were immersed in solution of Z907 dye for 18 h. Z907 dye was mixed at a concentration of 0.3 mM and dissolved in a solution of acetonitrile anhydrous to tert-butyl alcohol at equal volumetric ratio. For devices with ionic additives, HTM spiro-OMeTAD (Lumtec) as well as HTMs 1−3 (BASF) were dissolved in 0.17 mM chlorobenzene, 4-*tert*-butyl pyridine[19] (Sigma Aldrich), and 0.21 mM lithium bis(trifluoromethylsulfonyl)imide salt[20] (Sigma Aldrich) dissolved in anhydrous acetonitrile at 170 mg/mL mixed in a N_2 glovebox. Prior to spin coating, sensitized substrates were rinsed in a bath of acetonitrile, 25 μL of the hole-transporting material solution was cast onto the sensitized substrate and spun at a rate of 2000 rpm for 45 s. Cells were left in the dark in air overnight. To complete the device, 200 nm Ag electrodes were thermally evaporated. Samples for spectroscopic measurements were prepared in the same way in parallel to samples for device measurements. FTO was replaced by a quartz substrate and deposition of silver electrodes onto the sample was omitted. Spectroscopy samples were stored in a glovebox, in dark, until one hour prior to measurement.

Solar cell characterization was carried out by generating stimulated AM1.5G sunlight at 100 mW cm^{-2} irradiance using an AAB ABET technologies Sun2000 solar simulator calibrated with a silicon reference cell with a KG5 filter to minimize spectral mismatch. The mismatch factor was calculated to be less than 1%. JV curves were measured with a Keithley 2400 SourceMeter. The solar cells were masked with a metal aperture to define the active area and to minimize any edge effects and measured in a light-tight sample holder. The photovoltaic action spectra were taken using a Keithley 2400, with chopped monochromatic light incident on the masked solar cells.

UV−vis transmission spectra were collected using a Perkin-Elmer Lambda 9 UV−vis−NIR spectrophotometer with a dual beam setup.

Cyclic voltammetry experiments were performed under a nitrogen atmosphere using an Autolab PGSTAT12 potentiostat. Compounds were dissolved in a solution of 0.1 M tetrabutylammonium hexafluorophosphate in dichloromethane. A 3 mm glassy carbon working electrode was used with a Pt wire counter electrode and an Ag/AgNO3 reference electrode. The scan rate was 100 mVs^{-1}. All voltammograms were referenced to internal ferrocene (Fc/Fc^+ at 0 V).

Chemical oxidation of the hole-transporting materials was performed by dissolving each hole-transporting material in a 1:1 volume ratio mixture of acetonitrile and chlorobenzene with a molar concentration of 0.8 mM. Nitrosyl tetrafluoroborate ($NOBF_4$) 95% was purchased from Sigma Aldrich and dissolved in acetonitrile in molar concentrations of 25 and 250 mM. Increasing amounts of $NOBF_4$ were then added to the hole-transporting material solutions. During each step, 15 min after the injection of $NOBF_4$, UV−vis absorption measurements of the solutions were taken. Absorption spectra were later corrected for the dilution of the solution due to the addition of $NOBF_4$.

Field emission scanning electron microscopy (FESEM) images were obtained with a Hitachi S40300 operating at an accelerating voltage of 5 kV.

Photoinduced absorption spectra were obtained by photo-exciting with an argon ion laser tuned at 496.5 nm with a maximal power of 50 $\mu J \cdot cm^{-2}$ and chopped at a frequency of 23 Hz. The detection was made with a continuous white light probe (halogen bulb) of around 100 mW cm^{-2} intensity onto the sample. After passing through the sample, the probe beam enters a monochromator (SpectraPro-2300i, Acton Research Corporation) coupled to a diode for detection in the visible (PDA10A, Thorlabs) and in the NIR (ID-441-C, Acton Research Corporation). Acquisition was made by a lock-in amplifier locked at the light modulation frequency (SR830, Stanford Research Systems) and a NI USB-6008 (National Instruments) acquisition card.

Femtosecond transient absorption measurements were performed utilizing the output of a Ti:sapphire regenerative amplifier system with a pulse duration of 50 fs and a repetition rate of 1.1 kHz. The pump pulse was derived by feeding a fraction of the original pulse into an optical parametric amplifier (TOPAS) and using the output with a wavelength of 550 nm to excite the sample. The fluence was set to 50 $\mu J \cdot cm^{-2}$ for all measurements. The remaining fraction of the original beam was focused on a sapphire plate to generate a white light continuum pulse which was further split into a probe and a reference pulse to reduce the noise from variations in the beam intensity. The probe pulse was then passed through the excited part of the

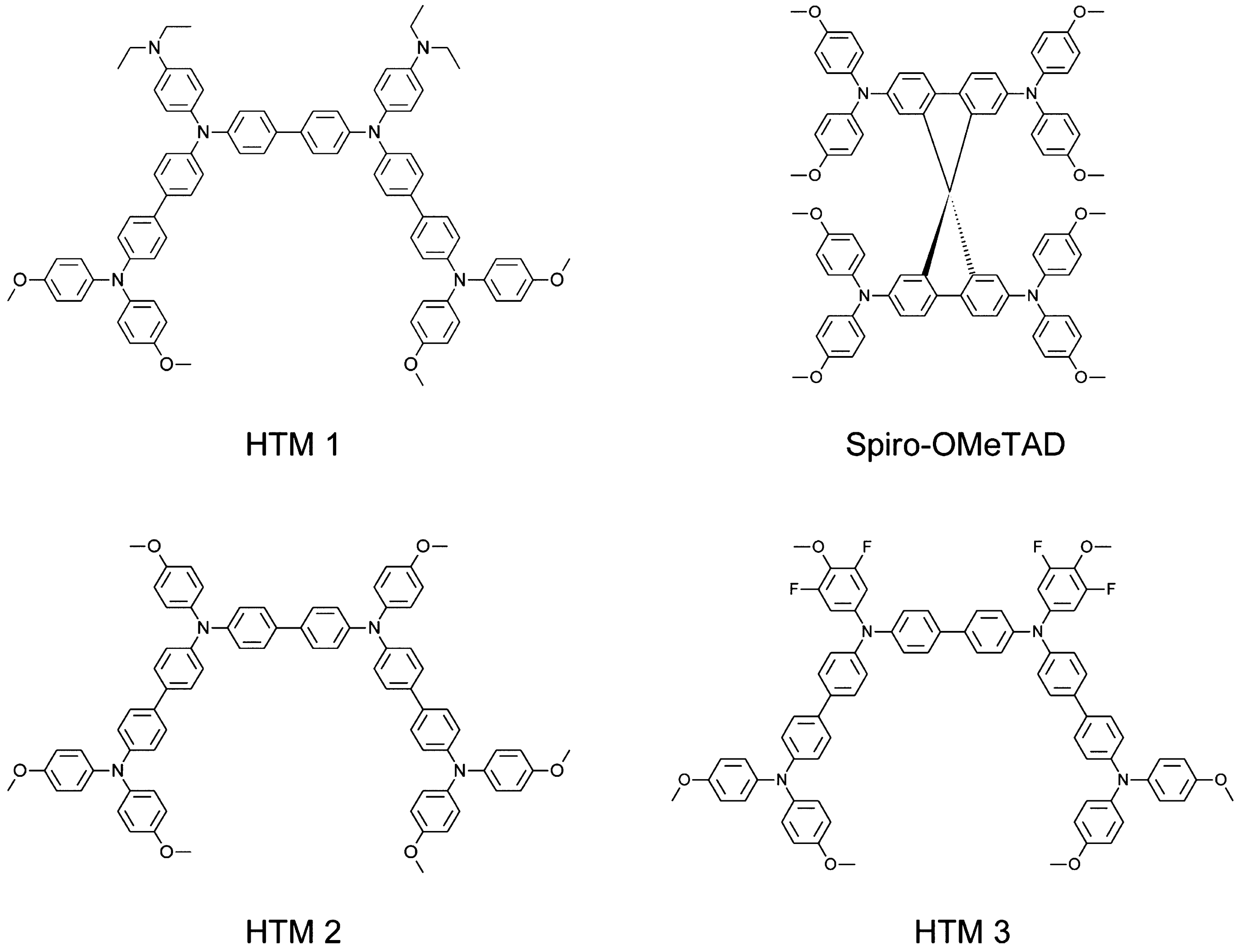

Figure 1. Chemical structures of the hole-transporting materials HTM **1**-**3** and the currently most widely employed HTM, spiro-OMeTAD, which is used as a reference in this study.

sample. In order to ensure a good spatial overlap, the size of the pump beam was set to about five times the size of the probe beam. Both probe and reference beams were filtered through either a 520 nm interference filter before being detected by two Si photodiodes coupled to an integrator and a lock-in amplifier. The signal was read out by triggering the lock-in amplifier with a signal from a chopper in the pump pulse set to 550 Hz creating a "pump-on", "pump-off" signal. The temporal delay between pump and probe pulse was varied by adjusting a mechanical delay stage.

Microsecond transient absorption spectroscopy was carried out using excitation pulses (550 nm, 7 ns pulse duration, 10 Hz repetition rate) produced by a Nd:YAG laser (EKSPLA, NT340) with a laser fluence on the sample maintained at 50 μJ/cm^2 per pulse. The probe light used in these experiments (520 nm) was produced by passing the output from a 150 W continuous wave xenon arc lamp through a monochromator (Acton Research Corporation, SpectraPro 2150i). The light transmitted through the sample was passed through a second monochromator (Acton Research Corporation, SpectraPro-2300i) before being detected by a fast photomultiplier tube module biased with 750 V (Hamamatsu, R9110). Data waves were recorded on an oscilloscope (Tektronix, DPO3054).

Transient photovoltage-photocurrent measurements were carried out using the setup described in detail elsewhere.[3,21−23] In short, the sample was biased with white light equivalent to 100 mW cm^{-2} solar illumination and perturbed with a red light pulsed diode. The perturbation was kept small enough to ensure that the voltage decay dynamics were approximately monoexponential. Photovoltage transients under short-circuit conditions are measured by holding the current generated by the white light bias fixed at J_{SC}. Since no extra current is allowed to flow as a result of the perturbation, the decay of the measured perturbation signal is a direct measure of the rate of charge recombination taking place within the device. Photocurrent transients at short-circuit are measured by holding the bias at 0 V, which allows charge transport to occur simultaneously with recombination. The decay rate, therefore, is a combination of recombination and transport rate. All decay curves were fitted with monoexponentials to estimate the decay rates.

In order to calculate the chemical capacitance (C) of the device, the total charge injected from the light pulse (ΔQ) is divided by the voltage perturbation (ΔV), i.e., $C = \Delta Q/\Delta V$. ΔQ is estimated by integrating the area under the measured current decay curve under short-circuit conditions. ΔV is extracted from the peak of the voltage perturbation under open-circuit conditions under the same bias light intensity.

Charge extraction measurements were performed by exposing the device to a constant white background light under short circuit conditions while the photocurrent response is measured with an oscilloscope. Once the device response is stabilized, the white background light is completely switched off and the subsequent photocurrent decay is measured. The charge density is then extracted by integrating the area under the curve for a known active area volume.

■ RESULTS AND DISCUSSION

Material Properties. Figure 1 shows the chemical structures of the three novel hole-transporting materials N^4,$N^{4\prime}$-([1,1′-biphenyl]-4,4′-diyl)bis(N^4-(4-(diethylamino)-phenyl)-$N^{4\prime}$,$N^{4\prime}$-bis(4-methoxyphenyl)-[1,1′-biphenyl]-4,4′-diamine) (**1**), N^4,$N^{4\prime}$-([1,1′-biphenyl]-4,4′-diyl)bis(N^4,$N^{4\prime}$,$N^{4\prime}$-tris(4-methoxyphenyl)-[1,1′-biphenyl]-4,4′-diamine) (**2**), and N^4,$N^{4\prime}$-([1,1′- biphenyl]-4,4′-diyl)bis(N^4-(3,5-difluoro-4-methoxyphenyl)-N^4,$N^{4\prime}$-bis(4-methoxyphenyl)-[1,1′-biphenyl]-4,4′-diamine) (**3**). Additionally, spiro-OMeTAD is shown which acts as a reference. HTM **1** differs from HTM **2** in that two methoxy groups were substituted by diethylamine groups. HTM **3** was derived from HTM **2** by fluorination of both carbon atoms ortho to the methoxy groups on two of the phenyl rings. All HTMs employ methoxy groups which have a high tendency to stabilize the radical cations due to their steric effect.[24]

Table 1 shows the characteristics of the aforementioned materials. HOMO levels were determined by solution-based cyclic voltammetry using the relationship $E_{\text{HOMO}}(\text{eV}) = -1.4E_{\text{onset,ox}}(\text{V}) - 4.6$[25] (see the Supporting Information). All materials have a similar molecular weight but differ in their HOMO energy levels. Comparing these to the dye Z907, the HTMs have an overpotential between 0.70 and 0.19 eV which is driving the hole-transfer process, although shifts in the dye oxidation potential of about 0.1−0.3 eV due to the adsorption to the TiO_2 surface are possible.[16,28,29] Assuming a minimum required overpotential of 0.2 eV,[2] we expect all HTMs, with the exception of HTM **3**, to have a large enough energy difference for hole-transfer yield close to unity. The overpotential of HTM **3** is approximately equal to the estimated minimum and could therefore result in incomplete hole transfer.

Table 1. Characteristics of the Hole-Transporting Materials Used in This Study^a

HTM	mol. weight (g/mol)	E_{HOMO} (eV)	overpotential (eV)	$E_{\text{opt,gap}}$ (eV)
HTM **1**	1237.57	−4.26	0.70	3.07
Spiro	1225.43	−4.52	0.44	2.99
HTM **2**	1155.38	−4.67	0.29	2.97
HTM **3**	1227.34	−4.77	0.19	2.88
Z907 dye	870.10	−4.96[27]		1.48

$^a E_{\text{HOMO}}(\text{eV}) = -1.4E_{\text{onset,ox}}(\text{V}) - 4.6$,[25] where $E_{\text{onset,ox}}$ was determined by solution-based cyclic voltammetry.[26] The optical bandgap E_{opt} was calculated from the absorption onset of the compound in solution.

Device Data. Table 2 summarizes the photovoltaic performance parameters for all HTMs in the presence of and in the absence of the standard additives 4-*tert*-butyl pyridine (tBP)[19] and lithium bis(trifluoromethylsulfonyl)imide salt (Li-TFSI).[20] While devices employing the new HTMs show a power-conversion efficiency close to zero in absence of the additives, spiro-OMeTAD reaches a value of about 1.3%. In presence of the additives, the efficiency of all devices increases substantially with a significant increase in the short-circuit current J_{SC} for all devices, in agreement with previous studies on liquid-electrolyte and solid-state DSSCs.[19,30−33] HTM **3** performed worst out of all devices and might have insufficient overpotential to drive the hole transfer process. Additionally, the efficiency of all new HTMs remained systematically below the efficiency of spiro-OMeTAD, with and without additives. When comparing the correlation and variation in power-conversion efficiency to that of the HOMO levels, no clear dependence is visible. This suggests that other parameters beyond the energy offset might play an important role for the efficiency.

Table 2. Photovoltaic Performance Parameters for the Studied Hole-Transporting Materials^a

HTM	η (%)	V_{OC} (V)	J_{SC}(mA cm^{-2})	FF
HTM **1**	0.01	0.56	0.13	0.11
spiro	1.26	0.65	3.28	0.59
HTM **2**	0.00	0.44	0.01	0.17
HTM **3**	0.08	0.63	0.49	0.25
HTM **1** + add.	1.40	0.70	3.99	0.50
spiro + add.	3.10	0.68	6.15	0.74
HTM **2** + add.	1.68	0.75	3.93	0.57
HTM **3** + add.	0.47	0.68	1.08	0.64

$^a\eta$, power-conversion efficiency; V_{OC}, open-circuit voltage; J_{SC}, short-circuit current; FF, fill factor. Results are presented for devices with and without the standard additives 4-*tert*-butyl pyridine (tBP) and lithium bis(trifluoromethylsulfonyl)imide salt (Li-TFSI).

Pore Filling. To determine the reason for the nonsystematic dependence on the HOMO level and the difference between the new HTMs and spiro-OMeTAD we compared the pore-filling fractions of all devices. As previously discussed, incomplete filling of the mesoporous network with the HTM is a limiting factor for the device performance.[14,34] There are two reasons for this. First, it hinders a complete regeneration of the dye in areas where no HTM molecules are present at the dye interface. Second, it prolongs the percolation path of the holes to the electrode therefore increasing the recombination probability.[11]

Several methods have been proposed to estimate the pore-filling fraction.[14,22,35,36] In one of these methods, the concentration of HTM in the porous network is estimated by adding the concentration in the pores before evaporation, which is given by the initial volume concentration c of the HTM solution, to the increase in concentration due to infiltration of HTM during the evaporation process.[22] The increase in concentration is calculated from the difference in HTM on top of the device before and after evaporation, divided by the volume of the pores given by the porosity p and the TiO_2 thickness d. While the amount of HTM on top of the device before evaporation can be calculated by the thickness d_{sol} of the solution and the concentration c, the amount of HTM after evaporation is given by the thickness d_{cl} of the capping layer. The pore-filling fraction is then given by[22]

$$\text{PFF} = c + \frac{d_{\text{sol}}c - d_{\text{cl}}}{dp} \tag{1}$$

To measure the thickness d_{cl} of the capping layer, we have taken SEM images of all devices, as shown in Figure 2. d_{sol} has

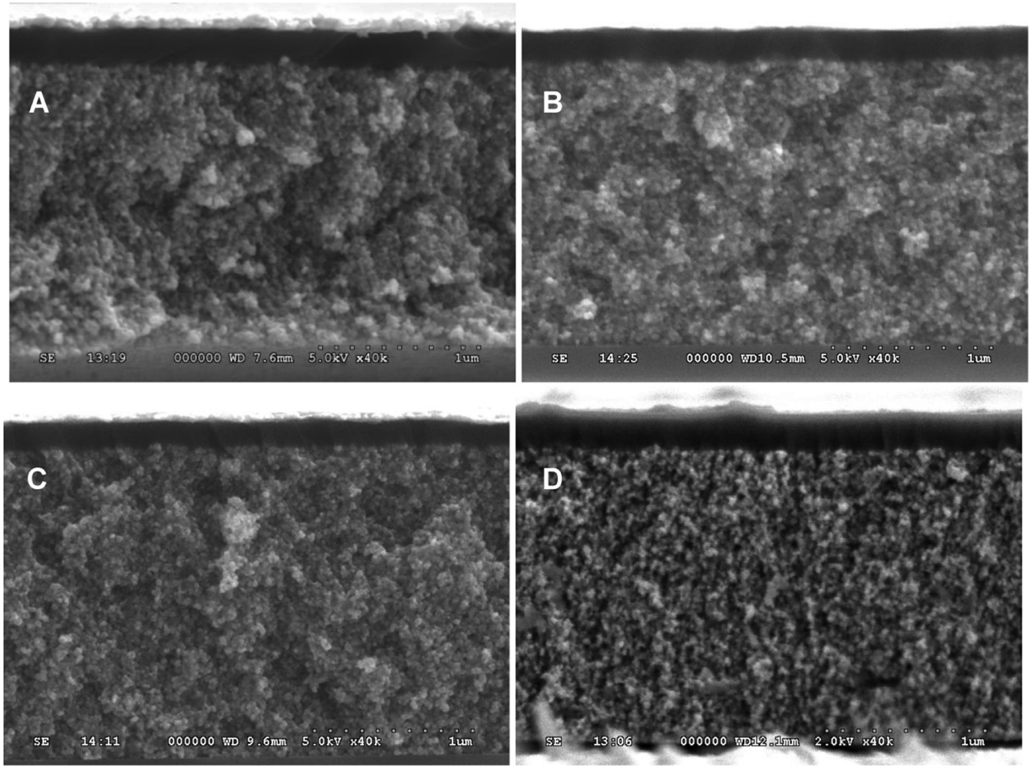

Figure 2. SEM images of devices consisting of TiO_2/Z907 and the hole-transporting material (A) HTM **1**, (B) spiro-OMeTAD, (C) HTM **2**, and (D) HTM **3**.

been measured to be 6.9 ± 0.5 μm for spiro-OMeTAD[14] and is assumed to be the same for all materials in this study. Using these values combined with a value of 49 ± 1%[14] for the porosity p and a concentration c of 10%, we estimate the pore-filling fractions to be between 60% and 70% for all HTMs. We thus observe no correlation between pore-filling fraction and device efficiency for the given samples. Since a pore-filling fraction of approximately 60% is estimated to be sufficient for optimized performance, we conclude that incomplete pore filling is not the main factor responsible for the differences in the power-conversion efficiency.[14]

Hole Transfer. Next, we used photoinduced absorption spectroscopy to study the efficiency of the hole-transfer process. To do this, we first chemically oxidized a solution of each HTM with nitrosonium tetrafluoroborate ($NOBF_4$), as shown in Figure 3a, to determine the absorption spectra of the radical cations. Spiro-OMeTAD has been well studied in the past and its radical cation spiro-OMeTAD$^+$ and its diradical cation spiro-OMeTAD^{2+} are known to show indistinguishable spectra with a peak around 511 nm and a shoulder around 700 nm, as well as a broad peak in the near-infrared.[22,37−39] Both HTM **2** and HTM **3** show similar peaks in comparison to spiro-OMeTAD, although the peak around 700 nm is stronger for HTM **3**. In contrast, HTM **1** shows a very broad peak spanning from the visible to the near-infrared.

With the absorption spectra of the radical cations known, the photoinduced absorption spectra of complete samples, which are shown in Figure 3b, can be interpreted. For a sample containing no HTM a negative feature is observed below 570 nm. This is attributed to photobleaching of the ground-state absorption of the dye caused by the presence of neutral or charged species.[40,41] For samples which include a HTM, the negative feature becomes smaller once hole-transfer from the dye to the HTM occurs as the photobleaching is reduced. Additionally, the signal is overlaid with the absorption of the radical cation on the HTM, as determined in Figure 3a. For all samples except the one containing HTM **3** hole transfer can be observed. Figure 3c shows the results for samples with additives. An increase in absorbance is visible for all HTMs at their respective absorption peaks. This indicates an increase in their long-lived charge density, except for HTM **3** which shows only a small change, in line with the previously observed small improvement of the power-conversion efficiency for the device (see Table 2). The poor efficiency of devices incorporating HTM **3** is therefore caused by the lack of long-lived radical cations on the hole-transporting material due to either fast recombination or poor hole-transfer yield.

To confirm these findings and to determine quantitatively the hole-transfer yield, we measured the hole-transfer dynamics using transient absorption spectroscopy. In this measurement, the dye is excited at a wavelength of 550 nm as it coincides with an absorption peak of Z907 and an absence of absorption from spiro-OMeTAD. The sample is then probed at 520 nm since all HTMs show absorption from the radical cations at this wavelength. Figure 4 shows the femto- to picosecond and micro- to millisecond dynamics. The initial negative signal is attributed to the photobleaching of the dye, whereas the ensuing signal is attributed to the absorption of radical cations on the HTM as well as the reduction of the photobleaching. The hole-transfer dynamics for spiro-OMeTAD show comparable dynamics to previous results in the literature where cis-$RuL_2(SCN)_2$ (where L is 4,4′-dicarboxy-2,2′-bipyridyl) was employed as a dye.[38] HTM **3** shows almost the same dynamics as the reference sample which does not have a HTM. Thus, very little hole transfer is present between Z907 and HTM **3**. In contrast, for HTM **1** and HTM **2** a hole-injection process is

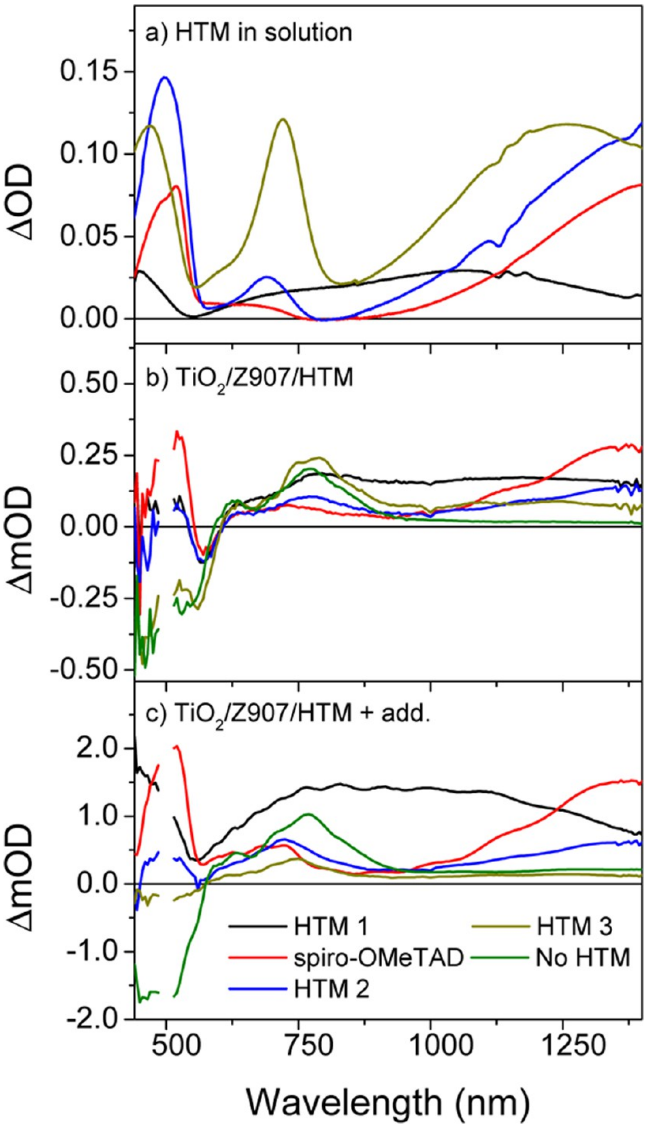

Figure 3. (a) UV−vis spectra of each hole-transporting material in acetonitrile and chlorobenzene (1:1) chemically oxidized with nitrosonium tetrafluoroborate ($NOBF_4$) at a molar ratio of 35%. (b) Photoinduced absorption spectra of TiO_2/Z907 samples with each hole-transporting material and a reference sample without a hole-transporting material. (c) Photoinduced absorption spectra of TiO_2/Z907 samples with each hole-transporting material prepared with the standard additives 4-*tert*-butyl pyridine (tBP) and lithium bis(trifluoromethylsulfonyl)imide salt (Li-TFSI) and one reference sample without a hole-transporting material. All samples were photoexcited at a wavelength of 496.5 nm.

clearly visible. Extrapolating the dynamics into the nano- to microsecond range, all HTMs complete the hole-transfer process within approximately 10 ns. Recombination, on the other hand, is not visible until approximately 2 μs. The time window between 1 and 2 μs can therefore be used to calculate the hole-transfer yields.

To relate the signal strength to the hole-transfer yield, the molar extinction coefficient of the HTMs (ε_{HTM+}) and the dye ($\varepsilon_{dye+} - \varepsilon_{dye0}$) need to be taken into account. The extinction coefficient of the ground state of Z907 at 520 nm has been found[41] to be approximately 12 000 L mol^{-1} cm^{-1}. In a careful study using chemical oxidation (see the Supporting Information), we determined the extinction coefficient of the spiro-OMeTAD radical cation to be approximately 26800 L mol^{-1} cm^{-1} at 520 nm, slightly higher than a previous value in the literature.[42] For HTM **1**-**3** the molar extinction coefficients at 520 nm are 2800, 20 300, and 7400 L mol^{-1} cm^{-1}, respectively. The hole-transfer yield is then calculated by comparing the signal strength of the ground-state bleaching (ΔOD_{dye}) to the signal strength of the sample with the HTM between 1 and 2 μs (ΔOD):[16,34,38]

$$\text{yield} = \left(1 - \frac{\Delta OD}{\Delta OD_{dye}}\right)\left(1 + \frac{\varepsilon_{HTM^+}}{\varepsilon_{dye^+} - \varepsilon_{dye^0}}\right)^{-1} \tag{2}$$

For spiro-OMeTAD, a value of approximately 75% is calculated.[43] For HTM **1**-**3** we estimate hole-transfer yields of approximately 100%, 46%, and 12%, respectively (see Figure 5). These results could potentially shift, if the signals started to decay at earlier times than the time resolution of our microsecond setup at 1 ns. However, for this deviation to occur the decay times of the ground-state bleaching and the HTM cation would also have to be substantially different as can be seen in eq 2. An introduction of an error due to a potential decay before 1 us seems therefore unlikely.

These hole-transfer yields can be related to the HOMO level of the HTM, as shown in Figure 5. Quantitatively, the dependence is given by the homogeneous thermodynamic equilibrium of holes in the HTM and in the dye.[16] However the results are much broader than what would be expected in this model. Haque et al.[16] suggested that the dependence is influenced by inhomogeneous broadening of the energy levels due to local variations in the energetics of the TiO_2/dye/HTM interface. Using this assumption, the data can be fitted with a midpoint of −4.63 eV and a full width at half-maximum (fwhm) of 0.33 eV, slightly lower than the value found in the aforementioned study. The midpoint of the fit is shifted by 0.33 eV compared to the HOMO level of Z907 (−4.96 eV[44]). This might be due to several reasons such as shifts in the dye oxidation potential resulting from adsorption to the TiO_2 surface[16,28,29] or differences in the cyclic voltammetry measurement techniques. Using the results from the model of inhomogeneous broadening, it can be seen that the energy offset between the dye Z907 and spiro-OMeTAD is close to optimal. Only small improvements of the power-conversion efficiency of solid-state DSSCs employing ruthenium based dyes are therefore expected when the HOMO level of the HTM is increased to deeper potentials. It is also estimated that an overpotential of approximately 180 meV should be sufficient to achieve a 90% efficient hole transfer. However, the intrinsic difficulties in determining the exact position of the energy levels of Z907 in the solid sensitized electrode leave quite significant ambiguity in the absolute energy alignment of dye and HTM HOMO levels. For example, the energy level alignment between the dye and the HTM may shift considerably upon physical contact, e.g., as a result of ground-state charge transfer. Additionally, after oxidation of the dye, the dye cation will have a much stronger oxidation potential in comparison to the neutral dye molecules. Hence, while Figure 5 provides an excellent picture of the changes with relative variation in HOMO level of the HTM, the absolute positioning of these energy levels will need to be determined with a higher degree of accuracy in future studies.

Charge Extraction. We now compare the hole transfer yields obtained for the different HTMs with the device short circuit currents in order to assess whether charge extraction

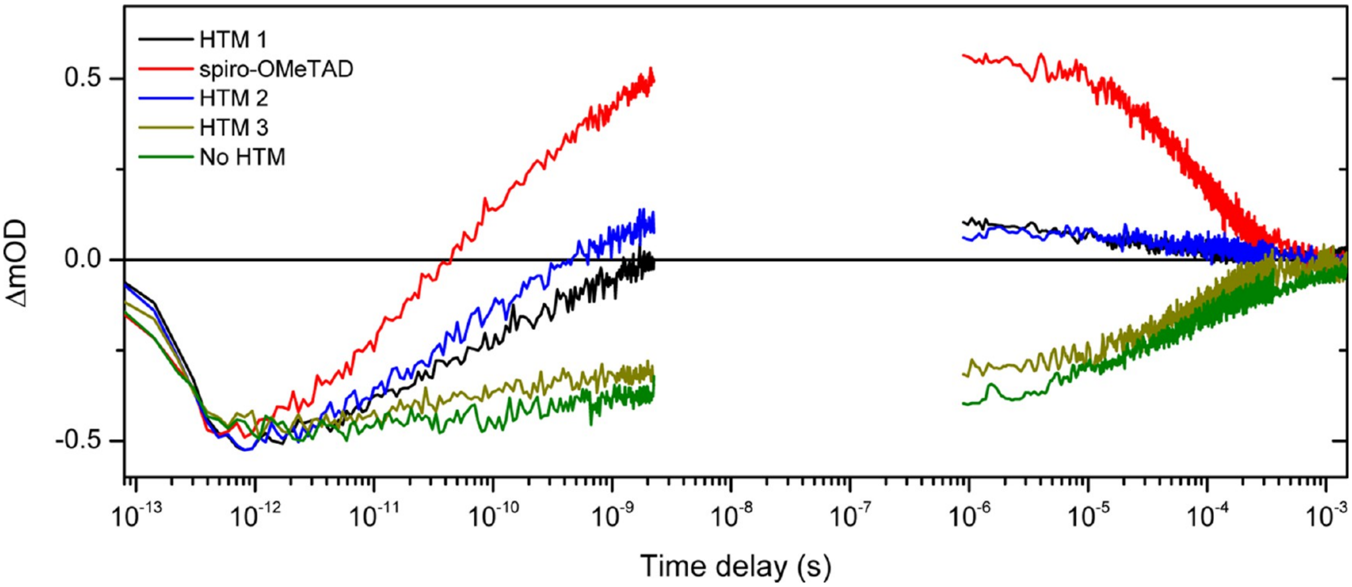

Figure 4. Transient absorption measurements of TiO_2/Z907 samples with the hole-transporting materials HTM **1** (black), spiro-OMeTAD (red), HTM **2** (blue), and HTM **3** (dark yellow) at a probe wavelength of 520 nm. Additionally, a TiO_2/Z907 sample without a hole-transporting material (green) is used as a reference. The samples were photoexcited at 550 nm with a fluence of 50 $\mu J/cm^2$. The micro- to millisecond transient absorption dynamics were scaled by a factor of 1.14 to allow for better comparison. The mismatch in the amplitude between the two time regimes is likely to be caused by a variation in fluence due to the use of two different experimental setups.

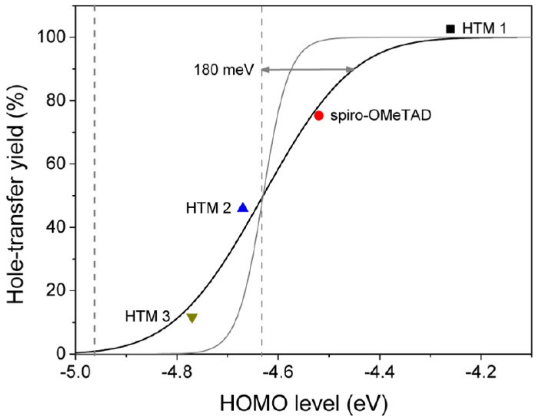

Figure 5. Dependence of the hole-transfer yield on the HOMO level of the hole-transporting material. The solid gray line is a fit assuming an inhomogeneous broadening, while the solid black line is a fit to the data based on a model assuming a Gaussian distribution for the local energy offsets between dye and hole-transporting material.[16] The gray dashed lines indicate the position of the Z907 HOMO level (−4.96 eV[44]) and the midpoint of the fit (−4.63 eV).

may also play a significant role on the overall device performance. The transient absorption experiments show that the deeper HOMO level of HTM **3** causes spiro-OMeTAD to have a 6.3 times higher hole-transfer yield than HTM **3**. Notably, the short-circuit current of the device containing spiro-OMeTAD is approximately 5.8 times higher than the device containing HTM **3**, as shown in Table 2. Since the short-circuit current is proportional to the hole-transfer yield and the difference in the power-conversion efficiency between the two devices is largely caused by different short-circuit currents, we can conclude that the poor performance of HTM **3** is mainly due to a very low hole-transfer yield between the dye and the HTM. Similarly, spiro-OMeTAD has a 1.6 times higher short-circuit current than **2** and shows a 1.6 times higher hole-transfer yield. The poor device performance of HTM **2** can thus be partially attributed to a reduced hole-transfer yield. HTM **1**, on the other hand, shows a higher hole-transfer yield than spiro-OMeTAD. The lower power-conversion efficiencies must therefore be due to other factors. To determine whether the inferior performance might be caused by a reduced charge-collection efficiency on the HTM or a negative influence of the electron injection into the TiO_2, we performed small-perturbation transient photovoltage-photocurrent measurements for devices illuminated with red light.[23,45] We observe the charge-collection efficiency through HTM **1**, HTM **2**, and spiro-OMeTAD to be the same (see the Supporting Information) and hole collection therefore cannot be responsible for the measured variations in device efficiency. In contrast, when measuring the capacitance as a function of the open-circuit voltage, we observe a clear shift of ~300 meV for the devices containing HTM **1** and HTM **2** in comparison to the device containing spiro-OMeTAD. Such an increase in the potential without significant change in the slope of the curve is consistent with a shift in the surface potential of the TiO_2. Such shifts will lower the density of states in the TiO_2 that are available for electron injection from the sensitizer.[45] We thus conclude that electron injection is partially inhibited in devices containing HTM **1** and HTM **2** in comparison to spiro-OMeTAD resulting in a lower electron extraction and hence device efficiency. The observed shift in surface potential may be caused either by direct interactions of the HTM with the TiO_2 electrode, or indirectly by the HTM arrangement, potentially due to crystallization of the HTM, influencing the distribution of ionic additives and thus creating a different ionic environment at the TiO_2 interface.

■ CONCLUSION

In summary, we compared three novel triarylamine type hole-transporting materials with varying HOMO levels to spiro-OMeTAD in order to explore the possibility of reducing the overpotential in order to improve the power-conversion efficiency. Using transient absorption spectroscopy, we estimated the hole-transfer yield of spiro-OMeTAD to be approximately 75%. This result shows that the energy alignment of spiro-OMeTAD is already close to optimal for ruthenium-based dyes leaving only small room for improvement. However the use of alternative HTMs such as HTM **2** and HTM **3** may prove to be advantageous for dye sensitizers with slightly different energy levels leading to better device performance than could be achieved when incorporating spiro-OMeTAD.

In addition, we found that all devices incorporating one of the new HTMs ultimately performed worse than those utilizing spiro-OMeTAD. While the difference in power-conversion efficiency of HTM **2** and HTM **3** in comparison to spiro-OMeTAD can partially be attributed to a lower hole-transfer yield caused by a smaller energy offset, HTM **1** showed a 100% hole-transfer yield and hence other factors must play a role. Using SEM imaging, we demonstrated that a pore-filling fraction of at least 60−70% is achieved by all HTMs and conclude that inferior pore filling is not limiting relative performance of devices incorporating the different HTMs. We further showed that devices containing HTM **1** and HTM **2** exhibit a shift of the TiO_2 surface potential toward a higher value which is likely to partially inhibit electron transfer from the dye into the TiO_2 limiting electron collection and device performance. Overall, our study shows that optimization of new hole transporters for solid-state DSCs involves a complex interplay of factors, including energy-level optimization, HTM pore infiltration, and HTM interactions with ionic additives and the TiO_2 surface.

■ ASSOCIATED CONTENT

Ⓢ Supporting Information

Chemical oxidation spectra and cyclic voltammetry graphs for all hole-transporting materials as well as charge-collection efficiency and capacitance measurements for complete devices. This material is available free of charge via the Internet at http://pubs.acs.org.

■ AUTHOR INFORMATION

Corresponding Author

*E-mail: l.herz1@physics.ox.ac.uk.

Notes

The authors declare no competing financial interest.

■ ACKNOWLEDGMENTS

The authors thank the Engineering and Physical Sciences Research Council for their financial support and BASF SE for providing the hole-transporting materials.

■ REFERENCES

(1) O'Regan, B.; Grätzel, M. A Low-Cost, High-Efficiency Solar-Cell Based on Dye-Sensitized Colloidal TiO_2 Films. *Nature* **1991**, *353*, 737−740.

(2) Hardin, B. E.; Snaith, H. J.; McGehee, M. D. The Renaissance of Dye-Sensitized Solar Cells. *Nat. Photonics* **2012**, *6*, 162−169.

(3) Tiwana, P.; Docampo, P.; Johnston, M. B.; Snaith, H. J.; Herz, L. M. Electron Mobility and Injection Dynamics in Mesoporous ZnO, SnO_2, and TiO_2 Films Used in Dye-Sensitized Solar Cells. *ACS Nano* **2011**, *5*, 5158−5166.

(4) Tiwana, P.; Parkinson, P.; Johnston, M. B.; Snaith, H. J.; Herz, L. M. Ultrafast Terahertz Conductivity Dynamics in Mesoporous TiO_2: Influence of Dye Sensitization and Surface Treatment in Solid-State Dye-Sensitized Solar Cells. *J. Phys. Chem. C* **2010**, *114*, 1365−1371.

(5) Nogueira, A. F.; Longo, C. Polymers in Dye Sensitized Solar Cells: Overview and Perspectives. *Coord. Chem. Rev.* **2004**, *248*, 1455−1468.

(6) Yella, A.; Lee, H. W.; Tsao, H. N.; Yi, C. Y.; Chandiran, A. K.; Nazeeruddin, M. K.; Diau, E. W. G.; Yeh, C. Y.; Zakeeruddin, S. M.; Grätzel, M. Porphyrin-Sensitized Solar Cells with Cobalt (II/III)-Based Redox Electrolyte Exceed 12% Efficiency. *Science* **2011**, *334*, 629−634.

(7) Bach, U.; Lupo, D.; Comte, P.; Moser, J.-E.; Weissörtel, F.; Salbeck, J.; Spreitzer, H.; Grätzel, M. Solid-State Dye-Sensitized Mesoporous TiO_2 Solar Cells with High Photon-to-Electron Conversion Efficiencies. *Nature* **1998**, *395*, 583−585.

(8) Burschka, J.; Dualeh, A.; Kessler, F.; Baranoff, E.; Cevey-Ha; Yi, C. Y.; Nazeeruddin, M. K.; Grätzel, M. Tris(2-(1H-pyrazol-1-yl)pyridine)cobalt(III) as p-Type Dopant for Organic Semiconductors and its Application in Highly Efficient Solid-State Dye-Sensitized Solar Cells. *J. Am. Chem. Soc.* **2011**, *133*, 18042−18045.

(9) Poplavskyy, D.; Nelson, J. Nondispersive Hole Transport in Amorphous Films of Methoxy-Spirofluorene-Arylamine Organic Compound. *J. Appl. Phys.* **2003**, *93*, 341−346.

(10) Kroeze, J. E.; Hirata, N.; Schmidt-Mende, L.; Orizu, C.; Ogier, S. D.; Carr, K.; Grätzel, M.; Durrant, J. R. Parameters Influencing Charge Separation in Solid-State Dye-Sensitized Solar Cells Using Novel Hole Conductors. *Adv. Funct. Mater.* **2006**, *16*, 1832−1838.

(11) Schmidt-Mende, L.; Grätzel, M. TiO_2 Pore-Filling and its Effect on the Efficiency of Solid-State Dye-Sensitized Solar Cells. *Thin Solid Films* **2006**, *500*, 296−301.

(12) Snaith, H. J.; Schmidt-Mende, L. Advances in Liquid-Electrolyte and Solid-State Dye-Sensitized Solar Cells. *Adv. Mater.* **2007**, *19*, 3187−3200.

(13) Schmidt-Mende, L.; Zakeeruddin, S. M.; Grätzel, M. Efficiency Improvement in Solid-State-Dye-Sensitized Photovoltaics with an Amphiphilic Ruthenium-Dye. *Appl. Phys. Lett.* **2005**, *86*, 013504.

(14) Docampo, P.; Hey, A.; Guldin, S.; Gunning, R.; Steiner, U.; Snaith, H. J. Pore Filling of Spiro-OMeTAD in Solid-State Dye-Sensitized Solar Cells Determined Via Optical Reflectometry. *Adv. Funct. Mater.* **2012**, *22*, 5010−5019.

(15) Garcia-Canadas, J.; Fabregat-Santiago, F.; Bolink, H. J.; Palomares, E.; Garcia-Belmonte, G.; Bisquert, J. Determination of Electron and Hole Energy Levels in Mesoporous Nanocrystalline TiO_2 Solid-State Dye Solar Cell. *Synth. Met.* **2006**, *156*, 944−948.

(16) Haque, S. A.; Park, T.; Holmes, A. B.; Durrant, J. R. Transient Optical Studies of Interfacial Energetic Disorder at Nanostructured Dye-Sensitised Inorganic/Organic Semiconductor Heterojunctions. *ChemPhysChem* **2003**, *4*, 89−93.

(17) Snaith, H. J. Estimating the Maximum Attainable Efficiency in Dye-Sensitized Solar Cells. *Adv. Funct. Mater.* **2010**, *20*, 13−19.

(18) Zakeeruddin, S. M.; Nazeeruddin, M. K.; Humphry-Baker, R.; Pechy, P.; Quagliotto, P.; Barolo, C.; Viscardi, G.; Grätzel, M. Design, Synthesis, and Application of Amphiphilic Ruthenium Polypyridyl Photosensitizers in Solar Cells Based on Nanocrystalline TiO_2 Films. *Langmuir* **2002**, *18*, 952−954.

(19) Krüger, J.; Plass, R.; Cevey, L.; Piccirelli, M.; Grätzel, M.; Bach, U. High Efficiency Solid-State Photovoltaic Device due to Inhibition of Interface Charge Recombination. *Appl. Phys. Lett.* **2001**, *79*, 2085−2087.

(20) Snaith, H. J.; Grätzel, M. Enhanced Charge Mobility in a Molecular Hole Transporter via Addition of Redox Inactive Ionic Dopant: Implication to Dye-Sensitized Solar Cells. *Appl. Phys. Lett.* **2006**, *89*, 262114.

(21) O'Regan, B. C.; Lenzmann, F. Charge Transport and Recombination in a Nanoscale Interpenetrating Network of n-Type and p-Type Semiconductors: Transient Photocurrent and Photovoltage studies of TiO2/dye/CuSCN photovoltaic cells. *J. Phys. Chem. B* **2004**, *108*, 4342−4350.

(22) Snaith, H. J.; Humphry-Baker, R.; Chen, P.; Cesar, I.; Zakeeruddin, S. M.; Grätzel, M. Charge Collection and Pore Filling

in Solid-State Dye-Sensitized Solar Cells. *Nanotechnology* **2008**, *19*, 424003.

(23) Docampo, P.; Guldin, S.; Stefik, M.; Tiwana, P.; Orilall, M. C.; Huttner, S.; Sai, H.; Wiesner, U.; Steiner, U.; Snaith, H. J. Control of Solid-State Dye-Sensitized Solar Cell Performance by Block-Copolymer-Directed TiO_2 Synthesis. *Adv. Funct. Mater.* **2010**, *20*, 1787−1796.

(24) Seo, E. T.; Nelson, R. F.; Fritsch, J. M.; Marcoux, L. S.; Leedy, D. W.; Adams, R. N. Anodic Oxidation Pathways of Aromatic Amines. Electrochemical and Electron Paramagnetic Resonance Studies. *J. Am. Chem. Soc.* **1966**, *88*, 3498−3503.

(25) D'andrade, B. W.; Datta, S.; Forrest, S. R.; Djurovich, P.; Polikarpov, E.; Thompson, M. E. Relationship between the ionization and oxidation potentials of molecular organic semiconductors. *Org. Electron.* **2005**, *6*, 11−20.

(26) Bredas, J. L.; Silbey, R.; Boudreaux, D. S.; Chance, R. R. Chain-Length Dependence of Electronic and Electrochemical Properties of Conjugated Systems - Polyacetylene, Polyphenylene, Polythiophene, and Polypyrrole. *J. Am. Chem. Soc.* **1983**, *105*, 6555−6559.

(27) Jennings, J. R.; Liu, Y.; Wang, Q.; Zakeeruddin, S. M.; Grätzel, M. The Influence of Dye Structure on Charge Recombination in Dye-Sensitized Solar Cells. *Phys. Chem. Chem. Phys.* **2011**, *13*, 6637−6648.

(28) Zaban, A.; Ferrere, S.; Gregg, B. A. Relative Energetics at the Semiconductor Sensitizing Dye Electrolyte Interface. *J. Phys. Chem. B* **1998**, *102*, 452−460.

(29) Planells, M.; Abate, A.; Hollman, D. J.; Stranks, S. D.; Bharti, V.; Gaur, J.; Mohanty, D.; Chand, S.; Snaith, H. J.; Robertson, N. Diacetylene Bridged Ttriphenylamines as Hole Transport Materials for Solid State Dye Sensitized Solar Cells. *J. Mater. Chem. A* **2013**, *1*, 6949−6960.

(30) Nazeeruddin, M. K.; Kay, A.; Rodicio, I.; Humphrybaker, R.; Muller, E.; Liska, P.; Vlachopoulos, N.; Grätzel, M. Conversion of Light to Electricity by cis-X2bis(2,2′-bipyridyl-4,4′-dicarboxylate)-ruthenium(II) Charge-Transfer Sensitizers (X = Cl-, Br-, I-, CN-, and SCN-) on Nanocrystalline Titanium Dioxide Electrodes. *J. Am. Chem. Soc.* **1993**, *115*, 6382−6390.

(31) Redmond, G.; Fitzmaurice, D.; Grätzel, M. Effect of Surface Chelation on the Energy of an Intraband Surface-State of a Nanocrystalline TiO_2 Film. *J. Phys. Chem.* **1993**, *97*, 6951−6954.

(32) Haque, S. A.; Park, T.; Xu, C.; Koops, S.; Schulte, N.; Potter, R. J.; Holmes, A. B.; Durrant, J. R. Interface Engineering for Solid-State Dye-Sensitized Nanocrystalline Solar Cells: The Use of Ion-Solvating Hole-Transporting Polymers. *Adv. Funct. Mater.* **2004**, *14*, 435−440.

(33) Haque, S. A.; Palomares, E.; Cho, B. M.; Green, A. N. M.; Hirata, N.; Klug, D. R.; Durrant, J. R. Charge Separation versus Recombination in Dye-Sensitized Nanocrystalline Solar Cells: The Minimization of Kinetic Redundancy. *J. Am. Chem. Soc.* **2005**, *127*, 3456−3462.

(34) Melas-Kyriazi, J.; Ding, I. K.; Marchioro, A.; Punzi, A.; Hardin, B. E.; Burkhard, G. F.; Tetreault, N.; Grätzel, M.; Moser, J.-E.; McGehee, M. D. The Effect of Hole Transport Material Pore Filling on Photovoltaic Performance in Solid-State Dye-Sensitized Solar Cells. *Adv. Energy Mater.* **2011**, *1*, 407−414.

(35) Cappel, U. B.; Gibson, E. A.; Hagfeldt, A.; Boschloo, G. Dye Regeneration by Spiro-MEoTAD in Solid State Dye-Sensitized Solar Cells Studied by Photoinduced Absorption Spectroscopy and Spectroelectrochemistry. *J. Phys. Chem. C* **2009**, *113*, 6275−6281.

(36) Ding, I. K.; Tetreault, N.; Brillet, J.; Hardin, B. E.; Smith, E. H.; Rosenthal, S. J.; Sauvage, F.; Grätzel, M.; McGehee, M. D. Pore-Filling of Spiro-OMeTAD in Solid-State Dye Sensitized Solar Cells: Quantification, Mechanism, and Consequences for Device Performance. *Adv. Funct. Mater.* **2009**, *19*, 2431−2436.

(37) Bach, U. Solid-State Dye-Sensitized Mesoporous TiO_2 Solar Cells. Ph.D. thesis; École Polytechnique Fédérale de Lausanne: Lausanne, Switzerland, 2000.

(38) Bach, U.; Tachibana, Y.; Moser, J.-E.; Haque, S. A.; Durrant, J. R.; Grätzel, M.; Klug, D. R. Charge Separation in Solid-State Dye-Sensitized Heterojunction Solar Cells. *J. Am. Chem. Soc.* **1999**, *121*, 7445−7446.

(39) Fantacci, S.; De Angelis, F.; Nazeeruddin, M. K.; Grätzel, M. Electronic and Optical Properties of the Spiro-MeOTAD Hole Conductor in Its Neutral and Oxidized Forms: A DFT/TDDFT Investigation. *J. Phys. Chem. C* **2011**, *115*, 23126−23133.

(40) Boschloo, G.; Hagfeldt, A. Photoinduced Absorption Spectroscopy of Dye-Sensitized Nanostructured TiO_2. *Chem. Phys. Lett.* **2003**, *370*, 381−386.

(41) Nazeeruddin, M. K.; Zakeeruddin, S. M.; Lagref, J. J.; Liska, P.; Comte, P.; Barolo, C.; Viscardi, G.; Schenk, K.; Grätzel, M. Stepwise Assembly of Amphiphilic Ruthenium Sensitizers and their Applications in Dye-Sensitized Solar Cell. *Coord. Chem. Rev.* **2004**, *248*, 1317−1328.

(42) In a previous study, a value of 18 700 L mol^{-1} cm^{-1} was found.[38,46] We assume that the difference is mainly due to reasons of concentration calibration and not due to differences during the chemical oxidation measurement.

(43) We note that previous studies found a hole-transfer yield of 90−100%.[10,38] The difference to the value of 75% found in this study is solely attributed to the assumption of a different molar extinction coefficent for spiro-OMeTAD radical cations at 520 nm, as detailed earlier.

(44) Mishra, A.; Pootrakulchote, N.; Wang, M. K.; Moon, S. J.; Zakeeruddin, S. M.; Grätzel, M.; Bauerle, P. A Thiophene-Based Anchoring Ligand and its Heteroleptic Ru(ii)-Complex for Efficient Thin-Film Dye-Sensitized Solar Cells. *Adv. Funct. Mater.* **2011**, *21*, 963−970.

(45) Tiwana, P.; Docampo, P.; Johnston, M. B.; Herz, L. M.; Snaith, H. J. The Origin of an Efficiency Improving Light Soaking Effect in SnO_2 Based Solid-State Dye-Sensitized Solar Cells. *Energy Environ. Sci.* **2012**, *5*, 9566−9573.

(46) Weissörtel, F. Amorphe, Niedermolekulare Ladungstransportmaterialien für Nanokristalline Solarzellen. Diplomarbeit, Universität Regensburg, 1996.